ACS APPLIED MATERIALS & INTERFACES

Research Article

www.acsami.org

Stretchable Thermoelectric Generators Metallized with Liquid Alloy

Seung Hee Jeong,*[,†] Francisco Javier Cruz,[†] Si Chen,[‡] Laurent Gravier,[§] Johan Liu,[‡] Zhigang Wu,[†,∥] Klas Hjort,[†] Shi-Li Zhang,[†] and Zhi-Bin Zhang*[,†]

[†]Department of Engineering Sciences, The Ångström Laboratory, Uppsala University, SE-751 21 Uppsala, Sweden

[‡]Department of Microtechnology and Nanoscience (MC2), Chalmers University of Technology, Kemivägen 9, SE-412 96 Gothenburg, Sweden

[§]Institute of Micro and Nano Techniques, University of Applied Sciences and Arts Western Switzerland, Yverdon-les-Bains CH-1401, Switzerland

[∥]State Key Laboratory of Digital Manufacturing Equipment and Technology, Huazhong University of Science and Technology, Wuhan 430074, China

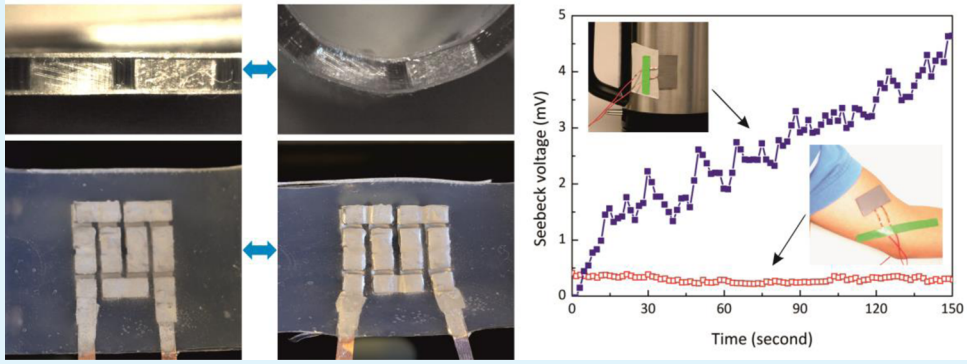

ABSTRACT: Conventional thermoelectric generators (TEGs) are normally hard, rigid, and flat. However, most objects have curvy surfaces, which require soft and even stretchable TEGs for maximizing efficiency of thermal energy harvesting. Here, soft and stretchable TEGs using conventional rigid Bi_2Te_3 pellets metallized with a liquid alloy is reported. The fabrication is implemented by means of a tailored layer-by-layer fabrication process. The STEGs exhibit an output power density of 40.6 $\mu W/cm^2$ at room temperature. The STEGs are operational after being mechanically stretched-and-released more than 1000 times, thanks to the compliant contact between the liquid alloy interconnects and the rigid pellets. The demonstrated interconnect scheme will provide a new route to the development of soft and stretchable energy-harvesting avenues for a variety of emerging electronic applications.

KEYWORDS: *stretchability, flexibility, thermoelectric generator, liquid alloy, interconnect, contact resistance, elastomer packaging*

1. INTRODUCTION

Soft and stretchable thermoelectric generators (STEGs) that are pliable to curvy and deformable surfaces are especially attractive for ubiquitous thermal energy harvesting.[1−5] One reason lies in the fact that an intimate physical contact between a TEG and a heat source surface is vital for minimizing thermal energy losses at the interface. Such a contact plays an increasingly crucial role in thermal energy harvesting from heat sources of curvy and deformable surfaces. The STEGs can be envisioned as unique power sources for variety of emerging devices, e.g., wearable, self-powered, mobile electronics;[6,7] skin electronics for human and robots;[8] and stretchable transducers[9,10] for the Internet of things. Development of the STEGs is in particular beneficial to the rapidly progressing field of soft robotics as a deformable energy source.[2,8] As a basic building block of soft and stretchable devices, stretchable conductors have been developed with metallic thin films in different special forms, e.g., meandering lines, springs, or metal fabrics.[11] Nanomaterial composites with carbon nanotubes and metallic nanowires have also been used as stretchable conductors.[12] Currently, mechanically flexible TEGs have been demonstrated on plastic foil substrates[5,13,14] using thermoelectric materials based on conducting polymers[13,15,16] or inorganic thin films.[17] Although mechanically bendable, they are not sufficiently adaptable to be conformal to and stay intimately on curvy or deformable surfaces. On the other hand, polymeric thermoelectric materials generally suffer from rather poor material efficiency characterized by the figure of merit ZT in the range of 1×10^{-5} to 0.4 primarily because of their rather low electrical conductivity.[15,16] Here, $ZT = (S^2\sigma T/k)$, where S is the Seebeck coefficient, σ the electrical conductivity, k the thermal conductivity, and T the absolute temperature,

Received: April 4, 2017
Accepted: April 24, 2017
Published: April 28, 2017

DOI: 10.1021/acsami.7b04752
ACS Appl. Mater. Interfaces 2017, 9, 15791−15797

respectively. In contrast, common Bi_2Te_3 has $ZT \sim 1$ when operated below 200 °C.[18] Recently, a wearable TEG has been reported with Bi_2Te_3/Sb_2Te_3 as thermoelectric materials printed on a glass fabric and packaged in a polydimethylsiloxane (PDMS) elastomer.[3] However, a real STEG that can reliably withstands large mechanical strains has not been demonstrated yet.

Meanwhile, a physical contact providing electrical and thermal connection is an important issue for interconnects of thermoelectric legs. Contacts easily degrade when subjected to mechanical strains as well as thermal stresses due to a mismatch of thermal expansion of heterogeneous materials during device operations. This leads to reduction of device efficiency and causes operational failures of a TEG. In addition, electrical ohmic contact and negligible thermal contact resistance are desired for minimizing unnecessary energy loss at interconnect contacts.[19−24]

In this work, we present a novel interconnect scheme for fabricating STEGs having high device efficiency. The scheme is implemented by using a Ga-based liquid alloy as an interconnect material which electrically wires Bi_2Te_3 pellets in series. An EcoFlex silicone elastomer with the Young's modulus of 30 kPa is applied as a packaging material.[25] The resultant STEGs exhibit an output power density from 19.8 to 40.6 $\mu W/cm^2$ when operated with 20 °C temperature difference across the devices at the average temperature of 25 °C. They can be stretched by at least 20%, and show excellent mechanical robustness and device operation reliability when subjected to stretching. Use of the EcoFlex elastomer makes the STEGs pliable to uneven and deformable surfaces as well as compatible with human skin.

2. EXPERIMENTAL SECTION

2.1. Materials. The elastomer (EcoFlex 00−30, Smooth-On) was prepared with 1:1 mixing ratio of a silicone base and a curing agent. The Ga-based liquid alloy (Galinstan, Geratherm Medical) was used as received. A thermal elastomer composite was prepared by mixing the silicone base and the curing agent of the elastomer, and the liquid alloy by a high speed mixing method. The liquid alloy was deposited by means of spraying with an air brush (Meec tools, Jula) connected to a pressure regulator (SL101−220, I&J Fisnar). Both p- and n-type Bi_2Te_3 pellets were used as received from European Thermodynamics, Ltd. Transparency films (Canon) were used as supporting substrate for processing and slide-glasses (VWR) were assembled to prepare a mold.

2.2. Design of STEGs. The basic structure of the STEGs was identical to the conventional one as illustrated in Figure 1a for a top view and Figure 1b for a cross-section view. P- and n-type Bi_2Te_3 pellets (2.8 mm × 2.8 mm in area and 1.15 mm in thickness) used as thermoelectric legs were alternatively connected in series via the Ga-based liquid alloy. The adjacent pellets were distanced by 1.0 mm. The liquid alloy interconnect was 2.8 mm in width and 100 μm in height. Both the pellets and the liquid alloy interconnects were embedded in the EcoFlex elastomer. The two outermost packaging layers between the liquid alloy interconnect and the environment consisted of either the same EcoFlex elastomer or a thermal elastomer composite. The latter composed of the EcoFlex elastomer and the liquid alloy fillers of 75 wt %.[26−28] Copper wires connected STEGs via the liquid alloy interconnects to an external characterization setup. The photograph in Figure 1c shows a typical STEG with 8 pairs of p- and n-type Bi_2Te_3 legs. The key steps for the STEG fabrication are illustrated in Figure 1d.

2.3. Fabrication Process of STEGs. The STEGs were fabricated by a layer-by-layer process. The process was started with laminating the EcoFlex elastomer prepolymer of 100 μm in thickness on a plastic substrate by using a film applicator (PA-2041, BYK-Gardner, GmbH)

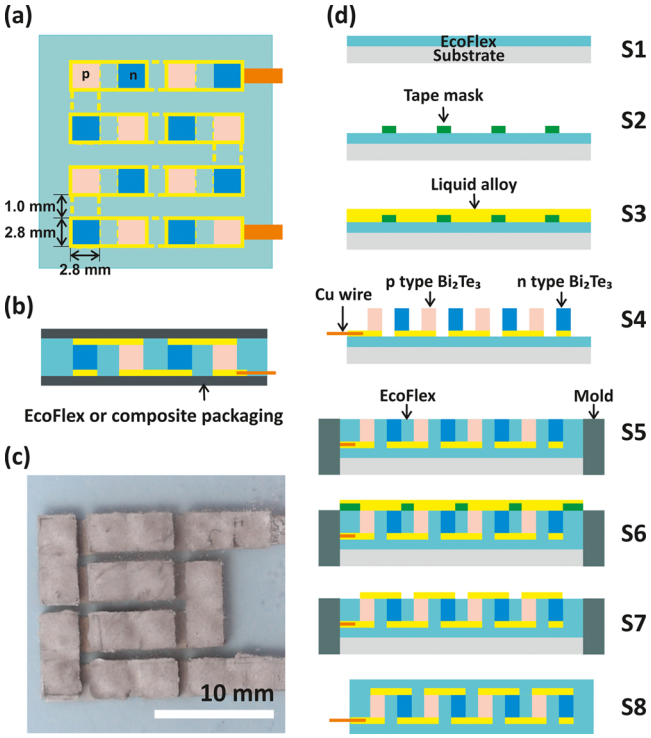

Figure 1. Schematic representation of STEG: (a) top view and (b) cross-section view. (c) Photograph of a fabricated 8-pair STEG. (d) Schematic illustration of the layer-by-layer fabrication process of STEGs.

(S1). The laminated elastomer layer was semicured in an oven at 75 °C. A tape mask was used during spraying to define the patterns of bottom interconnects (S2 to S3).[29] After removal of the masking tape, n- and p-type Bi_2Te_3 pellets were then placed alternatively on the liquid alloy interconnect patterns. The Bi_2Te_3 pellets, before being assembled, were coated with the liquid alloy on one side by spraying in order to ensure good wettability of the liquid alloy on the pellet surfaces. Copper wires were connected to the liquid alloy interconnects (S4). Using a slide glass mold, the EcoFlex prepolymer was filled in the mold until it reached the same height as the Bi_2Te_3 pellets (S5). After curing of the elastomer at 75 °C, the same patterning process as that bottom interconnect, i.e., from S2 to S3, was repeated in order to form the top liquid alloy interconnect (S6). It was followed by removal of the tape mask (S7). Laminating a top EcoFlex elastomer packaging layer was followed by curing. Finally, the support substrate was gently removed to complete the STEG fabrication (S8).

2.4. Measurement of Electrical and Thermal Properties. The electrical conductance of the p- and n-type Bi_2Te_3 pellets was measured using a standard four-probe measurement method with a semiconductor device analyzer (B1500A, Agilent Technologies). The thermal conductivity of the Bi_2Te_3 pellets, EcoFlex elastomer and thermal elastomer composite was measured by means of a Xenon flash method (NanoFlash, Netsch). The thermal resistance of a liquid alloy layer sandwiched between two Bi_2Te_3 pellets was measured in accordance to the ASTM D5470 standard method. The bond line thickness (BLT) of the liquid alloy layer between two Bi_2Te_3 pellets (7 mm × 7 mm in area, 1 mm in thickness) was measured using a displacement sensor unit (ZX-SF11, ZX-EDA41, Omron). Several layers of the liquid alloy of different thicknesses were prepared with different numbers of spacers. Each spacer was composed of a 70 μm thick vinyl tape between the Bi_2Te_3 pellets. The tape spacer was punched with a 5 mm diameter hole. Thermal resistance of the Bi_2Te_3 pellet was measured as a reference. Because the thermal conductivity of the spacer (<0.5 W/(m K)) was around 3 orders of magnitude lower than that of the liquid alloy, the influence of the spacer was negligible.

DOI: 10.1021/acsami.7b04752
ACS Appl. Mater. Interfaces 2017, 9, 15791−15797

2.5. Evaluation of Thermoelectric Generator Performance. Seebeck coefficients of the p- and n-type Bi_2Te_3 pellets, Seebeck voltage and output power of the STEGs were measured using a home-built thermoelectric measurement setup. The Seebeck coefficient of Bi_2Te_3 pellets were measured over 10 pellets of each type. The device performances were evaluated by measuring 3 or 4 STEGs for obtaining average values and error bar. The temperature was precisely controlled by a PID controller equipped with LabView (National Instruments). Thermocouples (K type, L221152−009, Pyro Controle), which were connected to a data acquisition unit (34972A, Agilent Technologies), were mounted inside the holes in two Cu blocks. The distance from the hole to the outer surface of the blocks was 500 μm. The generated voltage and power were measured under different temperature conditions with 0.05 °C accuracy. The temperatures of the Cu blocks were adjusted by Peltier elements (MCPF-127-14-25-E, Multicomp) connected to DC power supplies (6632B, Agilent technologies). A source-meter (SourceMeter 2400, Keithley) connected to the Cu blocks applied load current to the STEGs. All instruments and components were controlled by a LabVIEW program.

2.6. Measurement of Mechanical Reliability. Stretchability of the STEGs was evaluated on a home-built strain test setup equipped with a computer-controlled linear guide stage (Zaber Technology T-LSR300B). The change in resistance of the STEGs was recorded using a multimeter (34401A, Agilent technologies) during the cycling test. Delamination or fracture around embedded thermoelectric legs in the package was monitored under a microscope during the stretching test and after the cycling test. The stroke rate was 1 mm/sec.

3. RESULTS AND DISCUSSION

3.1. Electrical Contact Resistance between Liquid Alloy Interconnects and Bi_2Te_3 Pellets. When deposited by means of contact printing or drop casting, the liquid alloy did not wet easily on the Bi_2Te_3 pellets. We resolved this issue by spraying. A spraying process generates fine droplets which have relatively high momentum.[29] The energetic liquid alloy droplets impinged on the surface of Bi_2Te_3 pellets, and on the semicured elastomer prepared in a short processing time. As a result, the spraying process formed intimate contacts between the deposited liquid alloy and the surfaces of Bi_2Te_3 pellets as well as well-defined patterns of liquid alloy interconnects after the tape mask was removed. The quality of contacts was evaluated with a set of STEGs of 1, 4, 8 and 16-pair thermoelectric legs. It is noted that the spraying was performed in ambient, and the droplets shall contain a thin oxide layer on its surface. When the spraying was carried out in an environment of high HCl vapor pressure, poor wetting of the liquid alloy on pellets was observed. The HCl vapor was generated by placing drops of 1 M HCl close to the pellets in a fume hood. The HCl vapor etched the oxide layer on the surface of droplets. With a fresh surface of the droplets, the droplets did not stick to the pellets, and tended to merge and form larger size drops.

The generated power from an STEG depends on the electrical resistance and the thermal resistances of each component as well as to the various contact resistances in the module. The electrical resistance of an STEG mainly consists of the bulk resistance of Bi_2Te_3 pellets, electrical contact resistances between the liquid alloy/Bi_2Te_3, and the liquid alloy/Cu wires. Assuming that the liquid alloy interconnect has the same electrical contact resistance to both n- and p-type Bi_2Te_3 pellets, the total electrical resistance of an STEG, R_{STEG}, can be expressed as the following

$$R_{STEG} = n(4R_{c,LA\text{-}BiTe} + R_{n\text{-}BiTe} + R_{p\text{-}BiTe} + 2R_{LA}) + (2R_{c,LA\text{-}Cu} + 2R_{Cu} + R_{LA}) \quad (1)$$

where n is the number of Bi_2Te_3 pellet pairs, $R_{c,LA\text{-}BiTe}$ the contact resistance at the liquid alloy (LA)/Bi_2Te_3, $R_{c,LA\text{-}Cu}$ the contact resistance at the liquid alloy/Cu wire, $R_{n\text{-}BiTe}$ and $R_{p\text{-}BiTe}$ the bulk resistance of one n- and p-type Bi_2Te_3 pellet, respectively, R_{Cu} the resistance of the Cu wire, and R_{LA} the resistance of the liquid alloy. With the geometric dimensions given, the R_{LA} is 3.9×10^{-3} Ω using the electrical resistivity of 2.9×10^{-5} Ω cm.[30] By means of the van der Pauw measurement method, the electrical resistivity of a p- and an n-type Bi_2Te_3 pellet were obtained as 1.0×10^{-3} Ω cm and 1.2×10^{-3} Ω cm, respectively. This led to $R_{n\text{-}BiTe}$ of 1.8×10^{-4} Ω and $R_{p\text{-}BiTe}$ of 1.5×10^{-4} Ω for the pellets of the given dimensions. In Figure 2, it can be seen that R_{STEG} increased

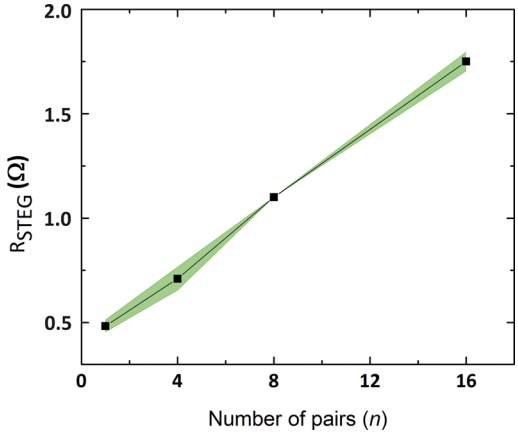

Figure 2. Total device resistance, R_{STEG}, as a function of the number of thermoelectric pairs, n. Experimental data average, dots; standard deviation, green colored region.

linearly as n increases. It should be noted that the Peltier effect and Joule heating during the resistance measurement by means of a multimeter is negligible since the measurement was performed in a short time at millisecond. From the slope of a linear fit to the experimental data points, $R_{c,LA\text{-}BiTe}$ of 19 mΩ was found. By neglecting any current crowding effect, the specific contact resistivity, ρ_C, became 1.5×10^{-3} Ω cm^2 for the liquid alloy/Bi_2Te_3 interface. This is 3−4 orders of magnitude higher than that of an ordinary contact between a solid metal and the Bi_2Te_3, i.e., 1×10^{-6} to 1×10^{-7} Ω cm^2. During the spraying of the liquid alloy, native oxide skin on the surface of a droplet instantly formed. Because ρ_C includes the contributions from the parts adjacent to the interface of the liquid alloy/Bi_2Te_3 pellet, the presence of the native oxide from every droplet most likely contributes to the specific contact resistivity.

3.2. Thermal Contact Resistance between Liquid Alloy Interconnects and Bi_2Te_3 Pellets. A thermal contact resistance gives rise to a temperature drop at the contacting interface and, as a result, deteriorates device efficiency. To estimate the level of thermal contact resistance between liquid alloy interconnects and Bi_2Te_3 pellets, we used the ASTM D5470 standard method[31] as shown in the inset of Figure 3a. This method led to a linear relation of the total thermal resistance R_{th} (Kmm^2/W) with the thickness of the liquid alloy. R_{th} consists of the thermal resistance with contribution of the liquid alloy and that of the two liquid alloy/Bi_2Te_3 contacts

DOI: 10.1021/acsami.7b04752
ACS Appl. Mater. Interfaces 2017, 9, 15791−15797

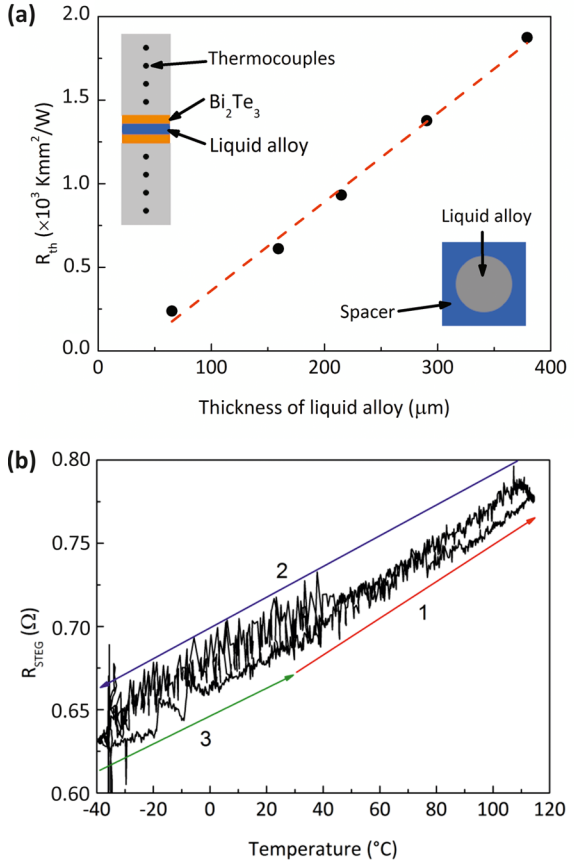

Figure 3. (a) Total thermal resistance, R_{th}, of the liquid alloy and the two liquid alloy/Bi_2Te_3 pellet interfaces as a function of the thickness of the liquid alloy with the cross-sectional view of the test structure illustrated as the upper-left inset and top-view as the lower-right inset. (b) Change in the total device resistance, R_{STEG}, of a 1-pair STEG with the variation of temperature during the first cycle of a thermal stress test.

($2R_{c,th}$). The latter, i.e., the thermal contact resistance, $R_{c,th}$, could be estimated by extrapolating R_{th} to zero thickness according to $R_{th} = 2R_{c,th} + t/k$, where t is the thickness and k the thermal conductivity of the liquid alloy.[32] It was found that $R_{c,th}$ is negligible for our STEGs within the resolution of the used method.

The thermal reliability of STEGs was examined by monitoring R_{STEG} of a 1-pair STEG in situ during thermally stressing in a testing chamber. In the first cycle of the thermal stress, as shown in the Figure 3b, R_{STEG} varied with the change of the temperature following the pathways from "1" to "3". The STEG showed a reversible behavior for the initial 4 cycles of thermal stress between −40 and 115 °C indicating good stability of the STEG including the liquid alloy/Bi_2Te_3 contacts. However, R_{STEG} was found to increase by a factor of ~30 from 0.6 Ω to 20 Ω at the room temperature after 300 cycles of the thermal stress as shown in Figure 3b. The mechanism behind the increase of R_{STEG} remains to be investigated.

3.3. Thermoelectric Power of STEGs. The variation of Seebeck voltage, V_S, of 1-pair STEGs as a function of ΔT at an average temperature of 25 °C is shown in Figure 4a, where ΔT is the temperature drop across the entire devices. The 1-pair STEG packaged in the EcoFlex elastomer generated ~3.0 mV with ΔT = 20 °C. As a comparison, V_S for an ideal 1-pair TEG, i.e., without elastomer packaging layers, was calculated according to $V_S = (S_p - S_n)\Delta T_{leg}$, where S_p (168 μV/K) and S_n (−166 μV/K) are the measured Seebeck coefficients of p- and n-type Bi_2Te_3 legs, respectively, and ΔT_{leg} is the temperature drop across the legs. For the same generated V_S, ΔT_{leg} in the ideal TEG is ~25% of the total ΔT in the fabricated ones. This can be explained by the fact that the EcoFlex elastomer has a very low thermal conductivity, i.e., 0.12 W/m K, which was measured at 25 °C by a Xenon flash method, and therefore, appreciable temperature drops across the packaging layers were created.

The variation of the output power, P, with the load resistance, R, is shown in Figure 4b for three STEGs of different n. R_{STEG} scaled linearly with n as described in eq 1. The result shows that P can be efficiently scaled up by increasing n. With the geometry that we used in this work, the power density reached 19.8 μW/cm^2, which corresponds to 1.0 μW/cm^2/°C, with ΔT = 20 °C at an average temperature of 25 °C.

By replacing the EcoFlex elastomer with the thermal elastomer composite for increased thermal conductivity, P was increased by a factor of 2 as shown in Figure 4c. In this case, the power density was 40.6 μW/cm^2, which corresponds to 2.0 μW/cm^2/°C. The thermal conductivity of the thermal elastomer composite is 0.28 W/m·K, about 2 times higher than that of the EcoFlex elastomer. As compared to the state of the art of flexible TEGs, this value is decent as shown in Table 1. It is noticed that there are differences in materials, structures of flexible TEGs, test setups and measurement conditions among the literatures and this work. The sizes of TEGs are estimated if not given in literatures. The current in relation with the voltage (I–V) is depicted in Figure 4d for 8-pair STEGs at various ΔT across the device. The electrical resistance of STEGs, which is determined by the slope of the curves, remained constant when ΔT varies.

Relative large variations of device characteristics can be observed in Figure 4. Even following the same procedure as described above, the fabricated STEGs varied in area and layer thickness of the interconnects and the packaging layers, contact resistances between the interconnects and TE legs, and material properties of the pellets. The contact between an STEG and Cu blocks of the measurement setup can also contribute to the performance variation.

3.4. Mechanical Stretchability and Reliability of STEGs. STEGs are soft and highly stretchable due to the use of the liquid alloy and the EcoFlex elastomer. Shown in Figure 5a, b is an 8-pair STEG with EcoFlex elastomer packaging at its as-made state and the stretched state, respectively. Although the sample was stretched by around 60% on the measurement setup, the strain of the active area in the device was 20%. The reduction of stretchability in the active area was mainly limited by the presence of rigid Bi_2Te_3 pellets although the liquid alloy and the EcoFlex elastomer were used. Compared to the use of meandering thin film metal interconnects, which require a sophisticated process to fabricate,[11] the liquid alloy does not need a special form, and can be implemented by a simple fabrication process. More importantly, a liquid alloy/Bi_2Te_3 interface is compliant, which is the key to the device reliability. The good adhesion of the soft EcoFlex elastomer to the rigid Bi_2Te_3 pellets prevented the liquid alloy from creeping along the interface. During the repeated operation of stretching and releasing for 1000 cycles, no delamination of the rigid Bi_2Te_3 pellets from the elastomer was observed. The variation in the electrical resistance of the STEG monitored in situ during the

DOI: 10.1021/acsami.7b04752
ACS Appl. Mater. Interfaces 2017, 9, 15791−15797

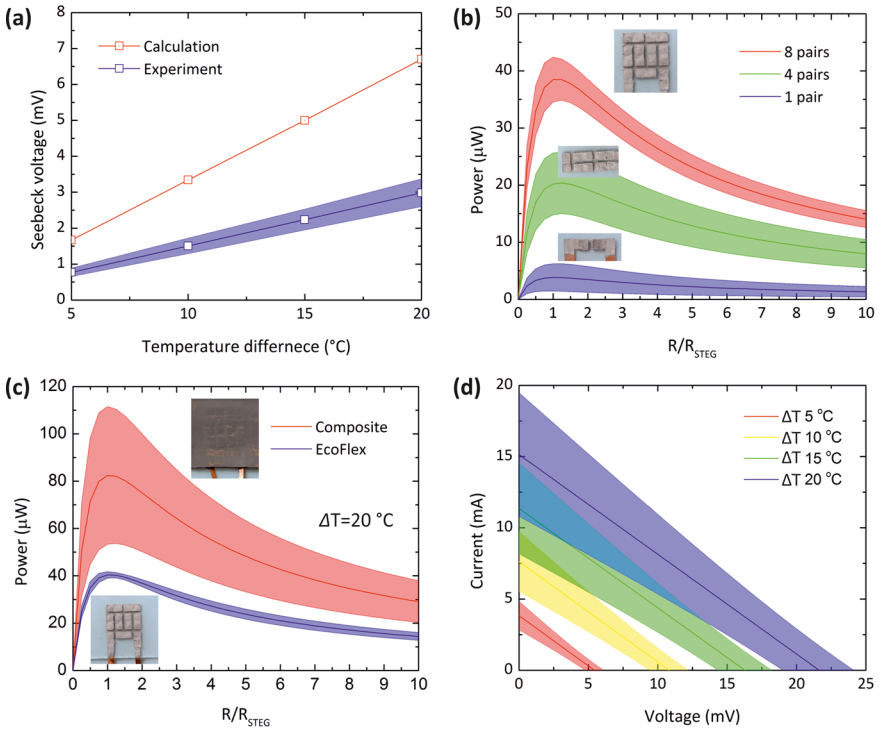

Figure 4. Thermoelectric performances of fabricated STEGs. (a) Seebeck voltage, V_S, measured on three 1-pair STEGs and calculated based on an ideal STEG model excluding packaging layers as a function of temperature difference ΔT, (b) variation of output power of STEGs of different number of pairs (n) with the ratio of load resistance (R) to device resistance (R_{STEG}) under ΔT = 20 °C across the devices and at an average temperature of 25 °C, (c) variation of output power with R/R_{STEG} for 8-pair STEGs with the EcoFlex elastomer and the thermal elastomer composite as the packaging material, and (d) current−voltage (I−V) of the 8-pair STEG with the thermal elastomer composite measured under various ΔT at an average temperature of 25 °C.

Table 1. Comparisons of Nonconventional TEGs

TEG	TE materials	legs (pairs)	area (mm^2)	ΔT (°C)	power density ($\mu W/mm^2/°C$)	interconnect	packaging	ref.
flexible	Bi_2Te_3/Sb_2Te_3	8	300	50	0.76	Cu	PDMS	3
flexible	Bi_2Te_3/Sb_2Te_3	100	832.4	40	9.6×10^{-7}	Au	Kapton	5
flexible	carbon nanotube/ polystylene	1985	1×10^4	70	7.8×10^{-4}	Au	polyethylene naphthalate	12
stretchable	n-/p-doped BiTe	8	201.6	20	0.02	galinstan	silicone composite	this work

mechanical strain cycling is shown in Figure 5c, with the first 10 cycles depicted as the inset for clarification. The R_{STEG} oscillated with the mechanical cycling, with amplitude around 10% of the initial value. A simple calculation showed that this resistance oscillation was most likely caused by the shape change of the liquid alloy resulting from mechanical pressure during cycling. Each cycle of mechanical strains led to a small decrease in the device resistance. After 1000 cycles, the total decrease of about 10% with respect to the initial value was found. This decrease is attributed to an improvement of the electrical contact of the liquid alloy to the Bi_2Te_3 pellets and to the Cu leads.

The advantage of the liquid alloy over solid metals for interconnects and contacts in STEGs is, hence, clear. The liquid alloy is compliant to large mechanical deformations and its use addresses the persistent challenge imposed by, e.g., thermal mismatch between solid metals and thermoelectric pellets in a conventional TEG. Because it remains liquid between −19 °C and 1300 °C, the liquid alloy allows our STEGs to operate reliably in the temperature range primarily set by the EcoFlex elastomer.

3.5. Applications. The softness and stretchability of STEGs further facilitated efficient energy harvesting of waste heat from objects with curvy and deformable surfaces. To demonstrate such unique and advantageous applications, an 8-pair STEG packaged with the thermal elastomer composite was applied onto the outer surface of an electric kettle, shown in the left inset of Figure 5d, and set on a human arm, shown in the right inset of Figure 5d. A continuous increase in V_S was recorded during heating up water in the former (solid square), whereas V_S remained nearly unchanged in the latter (open square). Although the bendability was primarily limited by the size of Bi_2Te_3 pellets, STEGs were found to be robust even when they were severely bent with a local radius as small as 10 mm.

4. CONCLUSIONS

In summary, we have demonstrated STEGs that were fabricated by utilizing Ga-based liquid alloy as interconnect, Bi_2Te_3 pellets as thermoelectric legs and elastomers as packaging. The liquid alloy provided a pliable contact to the STEGs and, as a result, enhanced device reliability. The fabrication process developed in this work represented a novel combination of laminating, spraying and molding. In particular, the use of spraying

DOI: 10.1021/acsami.7b04752
ACS Appl. Mater. Interfaces 2017, 9, 15791−15797

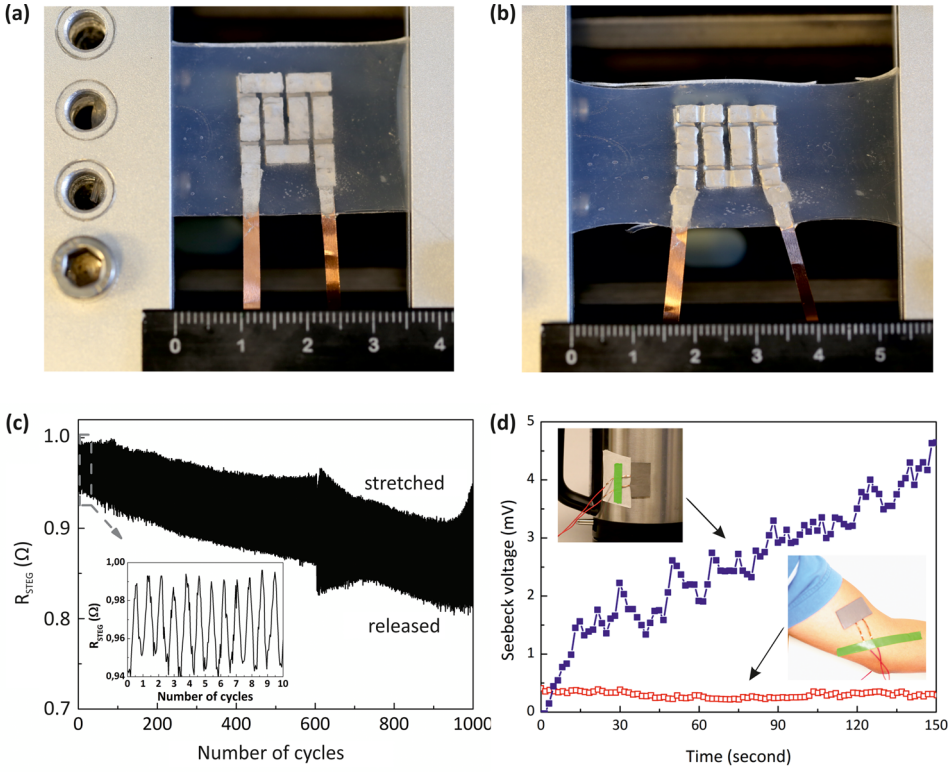

Figure 5. Mechanical stretchability and conformality of 8-pair STEGs. Photographs of a representative 8-pair STEG with EcoFlex elastomer packaging (a) without and (b) with mechanical stretching. (c) Variation in device resistance, R_{STEG}, with the number of cycles of the repeated mechanical stretching and releasing, with the first 10 cycles shown in the inset. (d) Change in Seebeck voltage, V_S, with time when an 8-pair STEG made with thermal elastomer composite packaging was attached to an electric kettle in operation (the upper-left inset) and on a human arm during walking (the lower-right inset).

technique ensured an intimate contact of the liquid alloy to the Bi_2Te_3 surface and a high-quality patterning of the liquid alloy. The STEGs generated 40.6 $\mu W/cm^2$ in power density with 20 °C temperature difference across the entire device at an average temperature of 25 °C, and showed excellent reliability and robustness under repeated mechanical strains. The realization of STEGs can pave the way for ubiquitous thermal energy harvesting of waste heat from objects that common solid-state TEGs are unthinkable to be directly applied to.

AUTHOR INFORMATION

Corresponding Authors

*E-mail: seunghee.jeong@angstrom.uu.se.

*E-mail: zhibin.zhang@angstrom.uu.se.

ORCID

Seung Hee Jeong: 0000-0003-0001-3197

Notes

The authors declare no competing financial interest.

ACKNOWLEDGMENTS

The authors are grateful to Malkolm Hinnemo for assistance in electrical measurement. This work was partially supported by the Swedish Foundation for Strategic Research (EM11-0002 and SE13-0061) and Swedish Research Council (621-2014-5596).

REFERENCES

(1) Rogers, J. A.; Someya, T.; Huang, Y. G. Materials and Mechanics for Stretchable Electronics. *Science* **2010**, *327*, 1603−1607.

(2) Bauer, S.; Bauer-Gogonea, S.; Graz, I.; Kaltenbrunner, M.; Keplinger, C.; Schwodiauer, R. 25th Anniversary Article: A Soft Future: From Robots and Sensor Skin to Energy Harvesters. *Adv. Mater.* **2014**, *26*, 149−161.

(3) Kim, S. J.; We, J. H.; Cho, B. J. A Wearable Thermoelectric Generator Fabricated on a Glass Fabric. *Energy Environ. Sci.* **2014**, *7*, 1959−1965.

(4) Francioso, L.; De Pascali, C.; Bartali, R.; Morganti, E.; Lorenzelli, L.; Siciliano, P.; Laidani, N. PDMS/Kapton Interface Plasma Treatment Effects on the Polymeric Package for a Wearable Thermoelectric Generator. *ACS Appl. Mater. Interfaces* **2013**, *5*, 6586−6590.

(5) Francioso, L.; De Pascali, C.; Farella, I.; Martucci, C.; Creti, P.; Siciliano, P.; Perrone, A. Flexible Thermoelectric Generator for Ambient Assisted Living Wearable Biometric Sensors. *J. Power Sources* **2011**, *196*, 3239−3243.

(6) Stoppa, M.; Chiolerio, A. Wearable Electronics and Smart Textiles: A Critical Review. *Sensors* **2014**, *14*, 11957−11992.

(7) Leonov, V.; Vullers, R. J. M.; Hoof, C. V. Thermoelectric Generator Hidden in a Shirt with a Fabric Radiator. *AIP Conf. Proc.* **2011**, *1449*, 556−559.

(8) Lu, N.; Kim, D. − H. Flexible and Stretchable Electronics Paving the Way for Soft Robotics. *Soft Robotics* **2014**, *1*, 53−62.

(9) Bauer, S.; Kaltenbrunner, M. Built To Disappear. *ACS Nano* **2014**, *8*, 5380−5382.

(10) Wu, Z. G.; Hjort, K.; Jeong, S. H. Microfluidic Stretchable Radio-Frequency Devices. *Proc. IEEE* **2015**, *103*, 1211−1225.

(11) Choi, S.; Lee, H.; Ghaffari, R.; Hyeon, T.; Kim, D.-H. Recent Advances in Flexible and Stretchable Bio-Electronic Devices Integrated with Nanomaterials. *Adv. Mater.* **2016**, *28*, 4203−4218.

(12) Chortos, A.; Bao, Z. Skin-inspired Electronic Devices. *Mater. Today* **2014**, *17*, 321−331.

DOI: 10.1021/acsami.7b04752
ACS Appl. Mater. Interfaces 2017, 9, 15791−15797

(13) Chen, Y.; Zhao, Y.; Liang, Z. Solution Processed Organic Thermoelectrics: Towards Flexible Thermoelectric Modules. *Energy Environ. Sci.* **2015**, *8*, 401−422.
(14) Suemori, K.; Hoshino, S.; Kamata, T. Flexible and Light Thermoelectric Generators Composed of Carbon Nanotube−Polystyrene Composites Printed on Film Substrate. *Appl. Phys. Lett.* **2013**, *103*, 153902−1−4.
(15) McGrail, B. T.; Sehirlioglu, A.; Pentzer, E. Polymer Composites for Thermoelectric Applications. *Angew. Chem., Int. Ed.* **2015**, *54*, 1710−1723.
(16) Kim, G. − H.; Shao, L.; Zhang, K.; Pipe, K. P. Engineered Doping of Organic Semiconductors for Enhanced Thermoelectric Efficiency. *Nat. Mater.* **2013**, *12*, 719−723.
(17) Fan, P.; Zheng, Z. − H.; Li, Y. − Z.; Lin, Q. − Y.; Luo, J. − T.; Liang, G. − X.; Cai, X. − M.; Zhang, D. − P.; Ye, F. Low-cost Flexible Thin Film Thermoelectric Generator on Zinc Based Thermoelectric Materials. *Appl. Phys. Lett.* **2015**, *106*, 073901−1−4.
(18) Minnich, A. J.; Dresselhaus, M. S.; Ren, Z. F.; Chen, G. Bulk Nanostructured Thermoelectric Materials: Current Research and Future Prospects. *Energy Environ. Sci.* **2009**, *2*, 466−479.
(19) Feng, S. P.; Chang, Y. H.; Yang, J.; Poudel, B.; Yu, B.; Ren, Z.; Chen, G. Reliable Contact Fabrication on Nanostructured Bi_2Te_3-based Thermoelectric Materials. *Phys. Chem. Chem. Phys.* **2013**, *15*, 6757−6762.
(20) Prem Kumar, D. S.; Mahajan, I. V.; Anbalagan, R.; Mallik, R. C. Design and Development of Thermoelectric Generator. *AIP Conf. Proc.* **2013**, *1591*, 628−630.
(21) Mishra, H.; Cola, B. A.; Rawat, V.; Amama, P. B.; Biswas, K. G.; Xu, X.; Fisher, T. S.; Sands, T. D. Thermomechanical and Thermal Contact Characteristics of Bismuth Telluride Films Electrodeposited on Carbon Nanotube Arrays. *Adv. Mater.* **2009**, *21*, 4280−4283.
(22) Gupta, R. P.; Xiong, K.; White, J. B.; Cho, K.; Alshareef, H. N.; Gnade, B. E. Low Resistance Ohmic Contacts to Bi_2Te_3 Using Ni and Co Metallization. *J. Electrochem. Soc.* **2010**, *157*, H666−670.
(23) da Silva, L. W.; Kaviany, M. Micro-thermoelectric Cooler: Interfacial Effects on Thermal and Electrical Transport. *Int. J. Heat Mass Transfer* **2004**, *47*, 2417−2435.
(24) Liu, W.; Wang, H.; Wang, L.; Wang, X.; Joshi, G.; Chen, G.; Ren, Z. Understanding of the Contact of Nanostructured Thermoelectric N-type $Bi_2Te_{2.7}Se_{0.3}$ Legs for Power Generation Application. *J. Mater. Chem. A* **2013**, *1*, 13093−13100.
(25) Menguc, Y.; Park, Y. − L.; Pei, H.; Vogt, D.; Aubin, P. M.; Winchell, E.; Fluke, L.; Stirling, L.; Wood, R. J.; Walsh, C. J. Wearable Soft Sensing Suit for Human Gait Measurement. *Int. J. Robot. Res.* **2014**, *33*, 1748−1764.
(26) Jeong, S. H.; Chen, S.; Huo, J.; Gravier, L.; Gamstedt, K.; Liu, J.; Zhang, S. L.; Zhang, Z. B.; Wu, Z. G.; Hjort, K. Thermal Elastomer Composites for Soft Transducers. In *18th International Conference on Solid-State Sensors, Actuators and Microsystems (TRANSDUCERS)*; Anchorage, AK, June 21−25, 2015 ; IEEE: Piscataway, NJ, 2015; pp1873−1876.
(27) Jeong, S. H.; Chen, S.; Huo, J.; Gamstedt, E. K.; Liu, J.; Zhang, S.-L.; Zhang, Z.-B.; Hjort, K.; Wu, Z. G. Mechanically Stretchable and Electrically Insulating Thermal Elastomer Composite by Liquid Alloy Droplet Embedment. *Sci. Rep.* **2016**, *5*, 18257.
(28) Bartlett, M. D.; Kazem, N.; Powell-Palm, M. J.; Huang, X.; Sun, W.; Malen, J. A.; Majidi, C. High Thermal Conductivity in Soft Elastomers with Elongated Liquid Metal Inclusions. *Proc. Natl. Acad. Sci. U. S. A.* **2017**, *114*, 2143−2148.
(29) Jeong, S. H.; Hjort, K.; Wu, Z. G. Tape Transfer Atomization Patterning of Liquid Alloys for Microfluidic Stretchable Wireless Power Transfer. *Sci. Rep.* **2015**, *5*, 8419.
(30) Liu, T.; Sen, P.; Kim, C. − J. Characterization of Nontoxic Liquid-metal Alloy Galinstan for Applications in Microdevices. *J. Microelectromech. Syst.* **2012**, *21*, 443−450.
(31) ASTM *D5470−12 Standard Test Method for Thermal Transmission Properties of Thermally Conductive Electrical Insulation Materials*; ASTM International: West Conshohocken, PA, 2012.
(32) Carlberg, B.; Ye, L. − L.; Liu, J. Polymer-Metal Nanofibrous Composite for Thermal Management of Microsystems. *Mater. Lett.* **2012**, *75*, 229−232.

DOI: 10.1021/acsami.7b04752
ACS Appl. Mater. Interfaces 2017, 9, 15791−15797